

Article

# $\mathcal{H}_2$ and $\mathcal{H}_\infty$ Optimal Control Strategies for Energy Harvesting by Regenerative Shock Absorbers in Cars <sup>†</sup>

Alessandro Casavola <sup>‡</sup>, Francesco Tedesco <sup>‡</sup> and Pasquale Vaglica <sup>\*</sup>

Modeling, Electronics and Systems (DIMES), Department of Informatics, University of Calabria, Via P. Bucci, 42/C, 87036 Rende (CS), Italy; a.casavola@dimes.unical.it (A.C.); ftedesco@dimes.unical.it (F.T.)

<sup>\*</sup> Correspondence: pasquale.vagl@gmail.com

<sup>†</sup> This paper is an extended version of our paper published in 2020 IEEE American Control Conference, Denver, CO, USA, 1–3 July, 2020.

<sup>‡</sup> These authors contributed equally to this work.

Received: 17 April 2020; Accepted: 20 May 2020; Published: 22 May 2020



**Abstract:** Regenerative suspension systems, unlike traditional passive, semi-active or active setups, are able to convert the traditionally wasted kinetic energy into electricity. This paper discusses flexible multi-objective control design strategies based on LMI formulations to suitably trade-off between the usual road handling and ride comfort performance and the amount of energy to be harvested. An electromechanical regenerative vehicle suspension system is considered where the shock absorber of each wheel is replaced by a linear electrical motor which is actively governed. It is shown by simulations that multivariable centralized control laws designed on the basis of a full-car model of the suspension system are able to achieve larger amount of harvested energy under identical ride comfort prescriptions with respect to scalar decentralized control strategies, designed on the basis of a single quarter-car model and implemented independently on each wheel in a decentralized way. Improvements up to 40% and 20% of harvested energy are respectively achievable by the centralized multivariable  $H_2$  and  $H_\infty$  optimal controllers under the same test conditions.

**Keywords:** regenerative shock absorbers; energy harvesting; active control of automobile suspension systems

---

## 1. Introduction

Research on regenerative suspension systems has gained increasing interest in recent years for the potential energy savings achievable in implementing active control strategies that ensure enhanced dynamic performance and the ability to convert wasted kinetic energy in electrical power for both energy harvesting and self-powered implementation. The state-of-the-art in the field has been recently reviewed in [1,2].

In a typical regenerative setup the viscous shock absorber is usually replaced by an electrical actuator that can be regulated to mimic a standard shock absorber (virtual shock absorber) or to provide a more general dynamical behavior in order to better trade-off between the conflicting requirements of harvesting large amounts of energy and ensuring good road handling and ride comfort performance.

In [3] a multiobjective  $H_\infty$  control design methodology has been recently proposed for actively regulating regenerative suspension systems and it was shown to be much more flexible in trading-off

among conflicting requirements and capable to dramatically improve the amount of harvested energy with respect to PI controllers implementing virtual shock absorbers where the only design knob is the dumping parameter.

The specificity of the control strategy proposed in [3], there referred to as Maximum Induced Power Control (MIPC) strategy, is that it may directly consider the amount of energy to be harvested amongst its objectives. This is done by imposing a model-reference prescription in closed-loop to the kinetic energy coming from the road that makes it arbitrarily large and sign-defined. The rationale is that, in the average, the amount of harvested electrical energy cannot be greater than the energy drained into the system from the road unevenness. Thus, maximizing the energy induced by the road and making it sign-defined may be a more effective control design objective in order to increase the amount of harvestable energy. Simulations and comparisons undertaken in [3] have confirmed the flexibility and the potentiality of the MIPC approach. A gain-scheduling version based on a LPV system formulation can be found in [4]. Similar conclusions on the superiority of the MIPC approach in terms of energy requirements for implementing the control strategy in comparison with standard passive control strategies were also drawn out in [5], where experimental comparisons of several control laws were undertaken on a lab regenerative shock absorber prototype.

One of the limitations of the MIPC approach described in [3] is that it is based on a quarter-car model and is limited to regulate the behavior of the regenerative suspension system of a single wheel. This approach obviously produces sub-optimal results because the four MIPC control laws are individually applied to the four wheels of the vehicles in a decentralized way, and the pitch and roll motions have not directly been taken into account in the design phase. As a consequence, each regulated suspension has the same dynamic behavior and provides the same amount of energy. Then, the total amount is simply given by four times the energy harvested by a single wheel. This approach, although suboptimal, is anyway of interest here because it will be used as a baseline solution for comparison purposes.

The main contribution of this paper is to present complete multivariable centralized MIPC approach is presented for the four wheels of a vehicle based on a full-car model of the regenerative suspension system. Both multi-objective  $H_\infty$  and  $H_2$  state-feedback control strategies are presented based on standard LMI control design formulations. Dynamical output feedback control syntheses are also possible but the details are not presented here for space limitation.

A final example is provided where comparisons among the decentralized state-feedback  $H_\infty$  solution of [3], and the centralized state-feedback  $H_\infty$  and  $H_2$  solutions presented here are reported. From these simulations, as expected, it clearly results that the multivariable centralized  $H_\infty$  and  $H_2$  MIPC approaches proposed here overcome the decentralized implementation because of the better system description, the coordinated implementation of the four controllers and the extra degrees of freedom available for the optimization. Moreover, it is also found that the centralized  $H_2$  approach allows one to harvest larger amount of energy for the same ride comfort requirement than the  $H_\infty$  MIPC approaches.

## 2. The Model and the Overall Control Architecture

### 2.1. The Full-Car Regenerative Suspension Model

The full-car regenerative suspension schematic under consideration is depicted in Figure 1. In such a system, the passive viscous dampers, usually present in any passive suspension systems for all four wheels, are here replaced by electromechanical actuators that generate forces  $f_i(t)$ ,  $i = 1, \dots, 4$  so as to suitably dampen the vertical, pitch and roll motions of the car body.

The 7DOF mathematical model proposed in [6] is used here to describe the pitch  $\theta_s$  and roll  $\varphi_s$  rotational motions (with  $I_p$  and  $I_s$  the corresponding moments of inertia) and the vertical motion of the

sprung mass  $m_s$  along its center of mass  $z_s$ . They consist of the following coupled linear differential equations (the dependance on the time is omitted for simplicity)

$$I_r \ddot{\phi}_s = -k_f t_f (z_{s1} - z_{u1}) + k_f t_f (z_{s2} - z_{u2}) - k_r t_r (z_{s3} - z_{u3}) + k_r t_r (z_{s4} - z_{u4}) + t_f f_1 - t_f f_2 + t_r f_3 - t_r f_4 \tag{1}$$

$$I_p \ddot{\theta}_s = -k_f a (z_{s1} - z_{u1}) - k_f a (z_{s2} - z_{u2}) + k_r b (z_{s3} - z_{u3}) + k_r b (z_{s4} - z_{u4}) + a f_1 + a f_2 - b f_3 - b f_4 \tag{2}$$

$$m_s \ddot{z}_s = -k_f (z_{s1} - z_{u1}) - k_f (z_{s2} - z_{u2}) - k_r (z_{s3} - z_{u3}) - k_r (z_{s4} - z_{u4}) + f_1 + f_2 + f_3 + f_4 \tag{3}$$

where  $z_{ui}$ ,  $i = 1, \dots, 4$  denote the vertical motions of the four unsprung masses described by

$$m_{u1} \ddot{z}_{u1} = k_f (z_{s1} - z_{u1}) - k_{tf} (z_{u1} - z_{r1}) - f_1 \tag{4}$$

$$m_{u2} \ddot{z}_{u2} = k_f (z_{s2} - z_{u2}) - k_{tf} (z_{u2} - z_{r2}) - f_2 \tag{5}$$

$$m_{u3} \ddot{z}_{u3} = k_r (z_{s3} - z_{u3}) - k_{tr} (z_{u3} - z_{r3}) - f_3 \tag{6}$$

$$m_{u4} \ddot{z}_{u4} = k_r (z_{s4} - z_{u4}) - k_{tr} (z_{u4} - z_{r4}) - f_4 \tag{7}$$

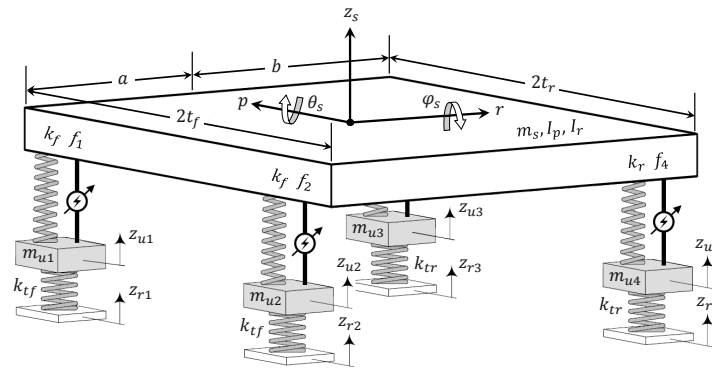


Figure 1. Full-car schematic for a regenerative setup.

In the above equations  $m_{u1}$  and  $m_{u2}$  represent the front wheels whereas  $m_{u3}$  and  $m_{u4}$  the rear ones, whose coupling with the road is simply modeled by the elastic stiffnesses  $k_{tf}$  and  $k_{tr}$  (for the front and rear couples of tires respectively). Moreover,  $k_f$  and  $k_r$  are the front and rear suspension stiffnesses respectively. Notice in particular that  $z_{si}$ ,  $i = 1, \dots, 4$  represent the vertical motions of the car body corners that, under a usual small pitch and roll angles assumption, are related to  $\phi_s$ ,  $\theta_s$  and  $z_s$  via the following linear expressions

$$z_{s1} = t_f \phi_s + a \theta_s + z_s \quad \dot{z}_{s1} = t_f \dot{\phi}_s + a \dot{\theta}_s + \dot{z}_s \tag{8}$$

$$z_{s2} = -t_f \phi_s + a \theta_s + z_s \quad \dot{z}_{s2} = -t_f \dot{\phi}_s + a \dot{\theta}_s + \dot{z}_s \tag{9}$$

$$z_{s3} = t_r \varphi_s - b\theta_s + z_s \quad \dot{z}_{s3} = t_r \dot{\varphi}_s - b\dot{\theta}_s + \dot{z}_s \tag{10}$$

$$z_{s4} = -t_r \varphi_s - b\theta_s + z_s \quad \dot{z}_{s4} = -t_r \dot{\varphi}_s - b\dot{\theta}_s + \dot{z}_s \tag{11}$$

Finally, the parameters  $a, b, t_f$  and  $t_r$  characterize geometrically the car body,  $z_{ri}, i = 1, \dots, 4$  denote the road profiles,  $z_{si} - z_{ui}, i = 1, \dots, 4$  the suspension strokes and  $z_{ui} - z_{ir}, i = 1, \dots, 4$  the tire deflections.

### 2.2. Power Flow Analysis

In order to arrive to consistent guidelines on how to maximize the harvested electrical power, a power flows analysis of the regenerative suspension system is accomplished in this subsection. To this end, with reference to Figure 1, one notes that the only exogenous signals that provide power to the regenerative suspension system are the four road profiles  $z_{ri}$  and no dissipative units, like viscous shock absorbers are present.

Then, by writing down the total energy  $E = K + V$  of the system, as the sum of the kinetic energy  $K$  of the masses and the potential energy  $V$  of the springs, one has

$$K = \frac{1}{2} I_r \dot{\varphi}_s^2 + \frac{1}{2} I_p \dot{\theta}_s^2 + \frac{1}{2} m_s \dot{z}_s^2 + \frac{1}{2} m_{uf} (\dot{z}_{u1}^2 + \dot{z}_{u2}^2) + \frac{1}{2} m_{ur} (\dot{z}_{u3}^2 + \dot{z}_{u4}^2) \tag{12}$$

$$V = \frac{1}{2} k_f [(z_{s1} - z_{u1})^2 + (z_{s2} - z_{u2})^2] + \frac{1}{2} k_r [(z_{s3} - z_{u3})^2 + (z_{s4} - z_{u4})^2] + \frac{1}{2} k_{tf} [(z_{u1} - z_{r1})^2 + (z_{u2} - z_{r2})^2] + \frac{1}{2} k_{tr} [(z_{u3} - z_{r3})^2 + (z_{u4} - z_{r4})^2] \tag{13}$$

Because power cannot be dissipated within the suspension system of Figure 1, it can only be exchanged with the road via its irregularities  $z_{ri}$  and with the electromagnetic devices via the exchanged forces  $f_i$ . In particular, such an exchanged power can be positive or negative. In fact, the road can introduce kinetic energy via the irregularities and absorbs part of the potential energy of the suspension during their discharging. On the other hand, the electromagnetic devices can act either as motors or generators by introducing or absorbing energy from the system.

Then, it makes sense to consider the power exchanged with the road  $P_s$  and the mechanical power exchanged with the actuators  $P_m$  and express the total instantaneous power  $\dot{E}$  in terms of the above two terms

$$\dot{E}(t) = P_s(t) + P_m(t) \tag{14}$$

By exploiting (1)–(7) and after direct mathematical manipulations one arrives to

$$\begin{aligned} \dot{E} = & -k_{tf} [(z_{u1} - z_{r1})\dot{z}_{r1} + (z_{u2} - z_{r2})\dot{z}_{r2}] - k_{tr} [(z_{u3} - z_{r3})\dot{z}_{r3} + (z_{u4} - z_{r4})\dot{z}_{r4}] \\ & + f_1(\dot{z}_{s1} - \dot{z}_{u1}) + f_2(\dot{z}_{s2} - \dot{z}_{u2}) + f_3(\dot{z}_{s3} - \dot{z}_{u3}) + f_4(\dot{z}_{s4} - \dot{z}_{u4}) \end{aligned} \tag{15}$$

and, on the basis of the above considerations, one can recognize that the power contribution from the road profiles and the actuators are clearly indetifiable

$$P_s(t) = -k_{tf} \sum_{j=1}^2 (z_{uj} - z_{rj})\dot{z}_{rj} - k_{tr} \sum_{j=3}^4 (z_{uj} - z_{rj})\dot{z}_{rj} \tag{16}$$

$$P_m(t) = \sum_{i=1}^4 f_i(\dot{z}_{si} - \dot{z}_{ui}) \tag{17}$$

As a result, as far as the exchanged power flows are concerned, the system can be considered as a series of two-port subsystems, as depicted in Figure 2, where the power  $P_s$  exchanged with the road acts at one terminal of the first subsystem, the mechanical power  $P_m$  is then exchanged with the electromechanical actuators that provide/request the electrical power  $P_e$ . In all terminals of the two-port systems we adopt the convention that the power is entering into the system when positive.

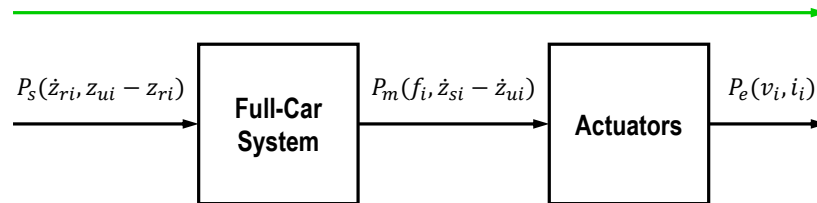


Figure 2. Power flows with the corresponding dual variables.

The above expressions for  $P_m$  and  $P_s$  generalized the ones achieved in [3] for a single regenerative suspension system derived from a quarter-car model and the same considerations can be drawn out here, briefly recalled hereafter for the reader convenience:

1. Ideally one would like to dispose of a control action capable to make both quantities large and sign defined for all time:

$$P_m(t) \ll 0, P_s(t) \gg 0 \text{ and } P_m(t) = -P_s(t), \tag{18}$$

If this were possible it would imply  $\dot{E}(t) = 0$ , which would ensure that the system has a perfect transfer of energy from the road to the electrical batteries.

2. Because  $f_i(t)$  are directly manipulable variables, it is quite easy to make  $P_m(t) < 0$  sign-defined. However,

$$\int_0^T |P_m(t)| dt \leq \int_0^T |P_s(t)| dt \tag{19}$$

expresses an obvious constraint on the energy that can be harvested in any interval  $[0, T]$  of interest, which cannot be larger than the energy provided by the road. Thus, it might make nonsense to try to maximize  $P_m$  by suitably design the control actions if  $P_s$  were small without disposing of any control degree of freedom to increase its amount any further.

3. Observe first that  $P_s$  is zero when the road profiles are all completely flat ( $\dot{z}_{ri} = 0, i = 1, \dots, 4$ ) or when the tire deflections are all zero, ( $z_{ui}(t) - z_{ri}(t) = 0$ ),  $i = 1, \dots, 4$ . Thus, high levels of energy harvesting on flat roads are incompatible with good road handling performance. From a control perspective, observe also that  $P_s$  depends on the regulated variables  $z_{ui}$ . Thus, if  $P_s$  were made sign-defined and as large as possible, viz.  $P_s \gg 0$  via a suitable control law this would increase the harvested energy regardless of the behavior (the sign) of  $P_m$ . Roughly speaking, making  $P_s > 0$  it would provide a barrier for the internal energy of the system from flowing back towards the road.

The above considerations were at the basis of the Maximum Induced Power Control (MIPC) decentralized design approach of [3] that will be extended here to the multivariable centralized case. It is expected that the more degrees of freedom arising in driving all four electromagnetic actuators by a single multivariable centralized controllers make easier the achievement of the above control requirements with respect to the use of four decentralized and no coordinated control actions.

### 2.3. Electromechanical Actuator Model

In this paper we consider four identical linear permanent-magnets electromechanical devices depicted in Figure 3 as a force actuators (LPMA) for the four wheels. Simple linear models of the generic LPMA actuator are given by

$$v_{ai}(t) = R_{ai}i_i(t) + L_{ai}\frac{di_i(t)}{dt} + K_i\dot{z}_i(t) \quad (20)$$

$$\dot{z}_i(t) = \dot{z}_{si}(t) - \dot{z}_{ui}(t) \quad (21)$$

$$f_i(t) = K_i i_i(t) \quad (22)$$

for  $i = 1, \dots, 4$  where  $f_i$  are the damping forces,  $i_i$  the armature currents,  $v_{ai}$  the armature voltages and  $\dot{z}_i$  the speed of the suspension stroke. The parameters  $R_{ai}$  and  $L_{ai}$  represent respectively the armature resistances and inductances while  $K_i$  are the force constants. The terms  $K_i\dot{z}_i(t)$  represent the back EMF voltages whereas the forces are proportional to the corresponding armature currents. The electrical power  $P_{ci}(t) = i_i(t)v_{ai}(t)$  results to be given by

$$P_{ci}(t) = R_{ai}i_i^2(t) + L_{ai}\frac{di_i(t)}{dt}i_i(t) + K_i\dot{z}_i(t)i_i(t), \quad (23)$$

where:  $P_{di} = R_{ai}i_i^2(t)$  represents the power dissipated by the Joule effect,  $P_{ci}(t) = L_{ai}\frac{di_i(t)}{dt}i_i(t)$  the electrical power stored in the inductance  $L_{ai}$  and  $P_{mi}(t) = K_i\dot{z}_i(t)i_i(t)$  the mechanical power acting on the  $i$ -th actuators. For a more accurate analysis of the dynamics of electromechanical devices well suited for energy harvesting purposes and their models see e.g., [7], where a discussion of the validity of assuming constant the coupling coefficients between the electrical and mechanical parts of the device is reported.

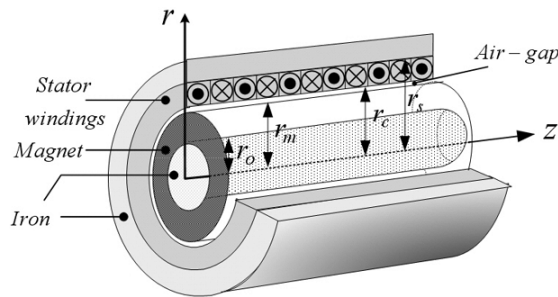


Figure 3. Permanent magnets linear electrical actuator.

Thus, Equation (23) suggests to work with electrical machines characterized by high voltages and low currents, in order to have small Joule losses and, in turn, a good efficiency. This requires actuators with large values of force constants  $K_i$  and small values for  $R_{ai}$ . Other losses are relevant only for high currents and are here neglected for simplicity.

### 2.4. The Overall Control Architecture

Figure 4 depicts the overall control architecture where two nested control loops are present. The inner one is governed by the *Current Controller* (CC) while the outer controller is termed *Regenerative Vibration Controller* (RVC) and it is in charge to provide the currents set-points to the inner CC controller.

The CC controller aims at regulating the armature current loops in the bank of four bidirectional DC-DC converters which establish the bidirectional electrical power flows between the battery and the four actuators. Its design is not considered here while we focus on the design of the RVC controller which is expected to provide the usual control performance of standard active suspension systems plus the ability to harvest as much energy as possible. Among many, for brevity, only optimal  $H_\infty$  and  $H_2$  centralized and decentralized static state-feedback control actions will be considered for the design of the RVC controller. Dynamic output feedback approaches will be considered in a future work.

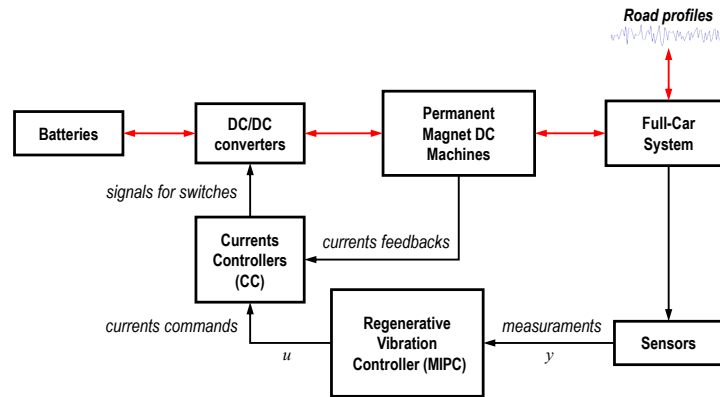


Figure 4. Overall control architecture.

### 3. RVC Control Design Specifications and LMI Based Designs

#### 3.1. Ride Comfort and Road Handling Control Specifications

Traditional control specifications in classical passive and active suspension systems mainly consists of finding a suitable trade-off between the *ride comfort* and *road handling* requirements, see e.g., [8,9].

Ride comfort is related to the passengers perception of vibrations at various frequency (0.5–80 Hz) that greatly depends on the capability of the suspension systems to attenuate the perceived acceleration levels as much as possible, especially at those frequencies more dangerous for the human body (0.5–5 Hz). Studies have shown that ride comfort may be directly related to sprung mass vertical accelerations  $\ddot{z}_s$  and/or  $\ddot{z}_{si}$ .

In order to avoid subjectivity, the ISO-2631 standard (see [10]) defines an index, referred to as the *Ride Index* (RI), that quantifies the human exposure to vibration by weighting the perceived acceleration by a human sensitivity curve defined by a band-pass filter:

$$Ride\ Index = \sqrt{a_{wx}^2 + a_{wy}^2 + a_{wz}^2} \tag{24}$$

$$a_{i,RMS} = \sqrt{\frac{1}{T} \int_0^T a_{wi}^2(t) dt} \quad i = x, y, z \tag{25}$$

where  $a_{wi}$  is the acceleration along the  $i$ -th axis weighed by the following filter:

$$W_k(s) = \frac{81.89s^3 + 796.6s^2 + 1937s + 0.14}{s^4 + 80s^3 + 2264s^2 + 7172s + 21196} \tag{26}$$

Lower values of the ride index imply better vibrations attenuation.

Road handling is another important objective, related to vehicle and passengers’ safety. It becomes extremely important in sportive/racing cars. It can usually be represented by the tire deflection  $z_u - z_r$  that has to be minimized in some norm.

### 3.2. Energy Harvesting Control Specification

A further requirement of a regenerative suspension system is that to harvest energy from the road unevenness. Based on the above considerations, this requirements is here optimized by making  $P_s$  sign-defined and as larger as possible.

This condition could be achieved by trying to enforce the following conditions on the tire deflections in closed-loop

$$z_{ui}(t) - z_{ri}(t) = -\alpha \dot{z}_{ri}(t), \quad i = 1, 2, 3, 4 \tag{27}$$

where  $\alpha > 0$  is a free constant design parameter. If all such conditions were satisfied for all time instants, the power  $P_s$  would result

$$\begin{aligned} P_s(t) &= - \left[ k_{tf} \sum_{j=1}^2 (z_{uj} - z_{rj}) \dot{z}_{rj} + k_{tr} \sum_{j=3}^4 (z_{uj} - z_{rj}) \dot{z}_{rj} \right] \\ &= \alpha k_{tf} (\dot{z}_{r1}^2(t) + \dot{z}_{r2}^2(t)) + \alpha k_{tr} (\dot{z}_{r3}^2(t) + \dot{z}_{r4}^2(t)) \end{aligned} \tag{28}$$

In this way, in principle,  $P_s(t)$  would be always positive (the power would always flow from the road to the suspension system) and large as desired by choosing a suitable large  $\alpha$ . However, it is worth pointing out that making the tire deflections large is in contrast with good road handling performance. Moreover, high levels of harvested energy require high armature currents that increase the electrical losses in the actuators. Then, depending on the application at hands, a suitable trade-off among the above conflicting control specifications has to be addressed in the design the RVC controller that can naturally formulated as a multi-objective optimal control design problem.

In fact, conditions (27) can be reformulated as the following model reference errors  $z_{pi}(t)$  to be minimized

$$z_{pi}(t) = z_{ui}(t) - z_{ri}(t) + \alpha \dot{z}_{ri}(t), \quad i = 1, 2, 3, 4 \tag{29}$$

### 3.3. State-Space Realization for the RVC Control Synthesis

Because the need of having a system description which uses the derivatives  $\dot{z}_{ri}$  instead of  $z_{ri}$  as exogenous signals for causally realizing  $z_{pi}$  in (29) we extend to the full-car case the alternative state-space representations used in [11,12] for the quarter-car model. The following state-space representation results

$$\dot{x}(t) = Ax(t) + Bu(t) + E\dot{z}_r(t) \tag{30}$$

corresponding to the following system vectors

$$x = \begin{bmatrix} z_{s1} - z_{u1} \\ z_{s2} - z_{u2} \\ z_{s3} - z_{u3} \\ z_{s4} - z_{u4} \\ \dot{\varphi}_s \\ \dot{\theta}_s \\ \dot{z}_s \\ z_{u1} - z_{r1} \\ z_{u2} - z_{r2} \\ z_{u3} - z_{r3} \\ z_{u4} - z_{r4} \\ \dot{z}_{u1} \\ \dot{z}_{u2} \\ \dot{z}_{u3} \\ \dot{z}_{u4} \end{bmatrix} \quad u = \begin{bmatrix} i_1 \\ i_2 \\ i_3 \\ i_4 \end{bmatrix} \quad \dot{z}_r = \begin{bmatrix} \dot{z}_{r1} \\ \dot{z}_{r2} \\ \dot{z}_{r3} \\ \dot{z}_{r4} \end{bmatrix} \tag{31}$$

for certain matrices  $A, B$  and  $C$  detailed in [13].

It is worth pointing out that the above state-space realization is not minimal in that the state has dimension 15 while the 7DOF full-car model (1)–(7) could be realized by a state of dimension 14. This choice is dictated by the greater easiness in specifying the various control objectives for the design of the controller that this realization offers.

The extra dimension has as a consequence that  $\text{rank}\{A\} = 14$ . In fact, it can be observed that  $A$  has one dominant real eigenvalue in zero and seven couple of pure imaginary conjugate eigenvalues. The eigenvalue in zero expresses the fact a linear combinations of state components remains constant during the free evolutions of the systems. In particular, it is found that the following linear dependence arises

$$t_r(z_{s1}(t) - z_{s2}(t)) - t_f(z_{s3}(t) - z_{s4}(t)) = 0, \forall t \tag{32}$$

along all the free evolutions of the system ( $z_{ri}(t) \equiv 0, i = 1, \dots, 4$ ). This condition trivially results by considering (8)–(11) and expresses the fact that in a rigid body the positions of three points are sufficient to characterize the positions of all other points of the body.

The state-space realization (30) is fully controllable. Thus, if the state is fully measurable ( $y(t) = x(t)$ ) linear state-feedback control laws can be freely designed. On the contrary, if only an output is available

$$y(t) = C_y x(t) + D_{yu} u(t) + D_{yw} z_r(t) \tag{33}$$

it is also full observable for many choices of sensors. For example, in [13] it is shown that the pair  $(A, C_y)$  corresponding to the following output

$$y = [z_{s1} - z_{u1} \quad z_{s2} - z_{u2} \quad z_{s3} - z_{u3} \quad z_{s4} - z_{u4} \quad \dot{z}_{s1} \quad \dot{z}_{s2} \quad \dot{z}_{s3} \quad \dot{z}_{s4}]^T \tag{34}$$

is full observable. In this second case, one has full freedom in designing any form of dynamic output feedback control laws.

Finally, for control design purposes it is convenient to introduce the following performance vector

$$z(t) = Cx(t) + Du(t) + F\dot{z}_r(t) \tag{35}$$

$$z = [\ddot{z}_{s1} \ddot{z}_{s2} \ddot{z}_{s3} \ddot{z}_{s4} i_1 i_2 i_3 i_4 z_{p1} z_{p2} z_{p3} z_{p4}]^T \tag{36}$$

where all conflicting objective variables of interest are considered. In particular,  $z(t)$  collects the four vertical accelerations  $\ddot{z}_{si}$  accounting for the drive comfort requirements, the four control actions  $i_i$  used to moderate the control energy so as to mitigate the electrical losses and the four variables  $z_{pi}$  defined in (29) related to the energy harvesting specifications. Again, details on the  $C$ ,  $D$  and  $F$  matrices can be found in [13].

### 3.4. Frequency Shaping of the State-Space Realization

A common practice in the design of optimal control laws is that of shaping the control objectives in frequency in order to penalize/enhance the performance in certain frequency bands of interest. This can be done by filtering the signals of the control systems.

By denoting with  $W_{ai}(s)$  the scalar, stable and proper filter shaping the vertical acceleration of the body corner  $\ddot{z}_{si}(t)$  and with  $W_{ui}(s)$  the one related to the current  $i_i(t)$ , the objective vector  $z(t)$  results filtered by the diagonal multivariable filter  $W_z(s)$  defined as:

$$W_z(s) = \text{diag} \{W_a(s), W_u(s), I_4\} \tag{37}$$

In particular, the aggregate filters  $W_a(s)$  e  $W_u(s)$  have the following structure

$$\begin{aligned} W_a(s) &= \text{diag} \{W_{a1}(s), W_{a2}(s), W_{a3}(s), W_{a4}(s)\} \\ W_u(s) &= \text{diag} \{W_{u1}(s), W_{u2}(s), W_{u3}(s), W_{u4}(s)\} \end{aligned} \tag{38}$$

and for simplicity are assumed identical

$$\begin{aligned} W_{a1}(s) &= W_{a2}(s) = W_{a3}(s) = W_{a4}(s) \\ W_{u1}(s) &= W_{u2}(s) = W_{u3}(s) = W_{u4}(s) \end{aligned} \tag{39}$$

It is convenient to select the  $W_{ai}(s)$  filters according to the ISO-2641 recommendations and using (26) to shape the accelerations in order to have the objectives directly related to the Ride Index. On the contrary,  $W_{ui}(s)$  are usually selected as high-pass filters in order to penalize the control actions at high frequency.

The energy of the road profiles are optionally shaped by a suitable bank of filters as well

$$W_d(s) = \text{diag} \{W_{d1}(s), W_{d2}(s), W_{d3}(s), W_{d4}(s)\} \tag{40}$$

$$W_{d1}(s) = W_{d2}(s) = W_{d3}(s) = W_{d4}(s) \tag{41}$$

Thus, by denoting with  $(A_z, B_z, C_z, D_z)$  e  $(A_d, B_d, C_d, D_d)$  the state-space representations of the filters  $W_z(s)$  and  $W_d(s)$ , with  $x_z$  and  $x_d$  the corresponding states, on the basis of the following extended state

$$x_g = [x^T \quad x_z^T \quad x_d^T]^T \tag{42}$$

one gets the extended state-space representation

$$\begin{cases} \dot{x}_g(t) = A_g x_g(t) + B_{gu}u(t) + B_{gw}\dot{z}_r(t) \\ \ddot{z}(t) = C_{gz}x_g(t) + D_{gzu}u(t) + D_{gzw}\dot{z}_r(t) \end{cases} \quad (43)$$

with

$$\begin{aligned} A_g &= \begin{bmatrix} A & \emptyset_{15 \times 20} & EC_d \\ B_z C & A_z & B_z FC_d \\ \emptyset_{4 \times 15} & \emptyset_{4 \times 20} & A_d \end{bmatrix} & B_{gu} &= \begin{bmatrix} B \\ B_z D \\ \emptyset_{4 \times 4} \end{bmatrix} \\ B_{gw} &= \begin{bmatrix} ED_d \\ B_z FD_d \\ B_d \end{bmatrix} & C_{gz} &= \begin{bmatrix} D_z C & C_z & D_z FC_d \end{bmatrix} \\ D_{gzu} &= D_z D & D_{gzw} &= D_z FD_d \end{aligned} \quad (44)$$

### 3.5. $H_2$ and $H_\infty$ Optimal State Feedback Designs

We assume hereafter that the state is measurable and that the system (43) is fully controllable. This happens to be true when no loss of controllability arises from the introduction of the shaping filters (poles/zeros cancellations). Thus, state-feedback control laws of the form

$$u(t) = Kx_g(t) \quad (45)$$

can be arbitrarily designed. In particular, the following closed-loop system results

$$\begin{cases} \dot{x}_g(t) = (A_g + B_{gu}K)x_g(t) + B_{gw}\dot{z}_r(t) \\ \ddot{z}(t) = (C_{gz} + D_{gzu}K)x_g(t) + D_{gzw}\dot{z}_r(t) \end{cases} \quad (46)$$

with

$$T(s) = (C_{gz} + D_{gzu}K)(sI - (A_g + B_{gu}K))^{-1}B_{gw} + D_{gzw} \quad (47)$$

being the closed-loop transfer matrix between  $\dot{z}(t)$  and  $\ddot{z}(t)$ .

#### 3.5.1. Optimal $H_\infty$ Control Synthesis

The  $H_\infty$  optimal state-feedback control law

$$u(t) = K_\infty x_g(t) \quad (48)$$

that minimizes the  $H_\infty$  norm of (47), that is

$$K_\infty := \arg \min_K \|T(s)\|_{H_\infty} \quad (49)$$

can be achieved by solving the following LMI optimization problem [14]

$$\begin{cases} \min_{X,Y,\gamma} \gamma \\ \text{s.t.} \\ \begin{bmatrix} A_{cl} + A_{cl}^T & B_{gzw} & (C_{gz}X + D_{gz}Y)^T \\ * & -\gamma I & D_{gz}^T \\ * & * & -\gamma I \end{bmatrix} < 0 \\ X = X^T > 0 \end{cases} \quad (50)$$

where  $A_{cl} := A_g X + B_{gu} Y$ . If the problem is feasible, the optimal  $H_\infty$  state-feedback gain is given by

$$K_\infty = YX^{-1} \quad (51)$$

### 3.5.2. Optimal $H_2$ Control Synthesis

The  $H_2$  optimal state-feedback control law

$$u(t) = K_2 x_g(t) \quad (52)$$

that minimizes the  $H_2$  norm of (47), that is

$$K_2 := \arg \min_K \|T(s)\|_{H_2}^2 \quad (53)$$

can be achieved by solving the following LMI optimization problem [14]

$$\begin{cases} \min_{X,Y,Q,\nu} \nu \\ \text{s.t.} \\ \begin{bmatrix} A_{cl} + A_{cl}^T & B_{gzw} \\ * & -I \end{bmatrix} < 0 \\ \begin{bmatrix} X & (C_{gz}X + D_{gz}Y)^T \\ * & Q \end{bmatrix} > 0 \\ X = X^T > 0 \\ Q = Q^T > 0 \\ Tr(Q) \leq \nu, \end{cases} \quad (54)$$

where  $A_{cl} := A_g X + B_{gu} Y$ . If the problem is feasible, the optimal  $H_2$  state-feedback gain is given by

$$K_2 = YX^{-1} \quad (55)$$

## 4. Simulation Results

Several Matlab/Simulink simulations have been undertaken for assessing the full-car  $H_2$  and  $H_\infty$  MIPC approaches presented here and compare them with the quarter-car  $H_\infty$  state-feedback solution described in [3]. The latter control law, designed for the suspension systems of a single wheel, will be then applied to all four suspension systems in a decentralized way.

The three control approaches, namely  $H_\infty$  decentralized,  $H_\infty$  centralized and  $H_2$  centralized, will be compared on the same car, actuators and driving scenario with the available design knobs tuned to achieve the same Ride Index for the three control strategies.

In particular, three values of the Ride Index will be considered:  $RI = 0.25$ ,  $RI = 0.47$  and  $RI = 0.70$  that, according to the ISO 2631 RI classification, correspond respectively to *not uncomfortable*, *a little uncomfortable* and *fairly uncomfortable* likely passengers reactions

Road’s profiles complying with the ISO-8608 standard [15] have been used in the simulations. In particular, all simulations have been undertaken by assuming to drive on a C straight road at 70 Km/h. Figure 5 depicts the corresponding profiles

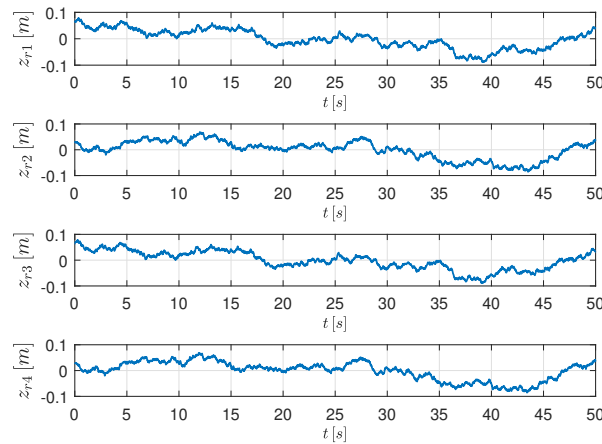


**Figure 5.** Road profiles  $z_{r1}(t)$ ,  $z_{r2}(t)$ ,  $z_{r3}(t)$  and  $z_{r4}(t)$  used in the simulations.

The same standard class-C vehicle and actuator considered in [3] (where all relevant parameters are listed) is used here.

The following dynamical weights have been used in the three control strategies

$$W_{ai}(s) = \rho W_k(s) \text{ (defined in (26))} \tag{56}$$

$$W_{ui}(s) = \beta \frac{s + 1}{s + 10} \tag{57}$$

$$W_{di}(s) = \gamma \frac{10}{s + 1000} \tag{58}$$

with  $\rho$ ,  $\beta$ ,  $\gamma$  and  $\alpha$  in (29) as free design knobs. The fact that the regulation of the Ride Index can be simply achieved by tuning the few control design knobs testifies favorably on the flexibility of the proposed MIPC approach.

#### 4.1. Simulations for Ride Index = 0.25

The values of design knobs values used in the  $RI = 0.25$  simulations are reported in Table 1 whereas the plots of the acceleration  $\ddot{z}_{s1}$ , actuation current  $i_1(t)$  and the harvested electrical power  $P_{e1}(t)$  under the three control laws are reported in Figure 6

**Table 1.** Knobs tuning—RI = 0.25.

RI = 0.25 (Excellent Comfort/Smallest Harvesting)				
Control	$\rho$	$\beta$	$\gamma$	$\alpha$
$H_{\infty,dec}$	0.2067	100	10	30
$H_{\infty,cen}$	0.42	3.45	1	27
$H_{2,cen}$	0.5	2	1	29

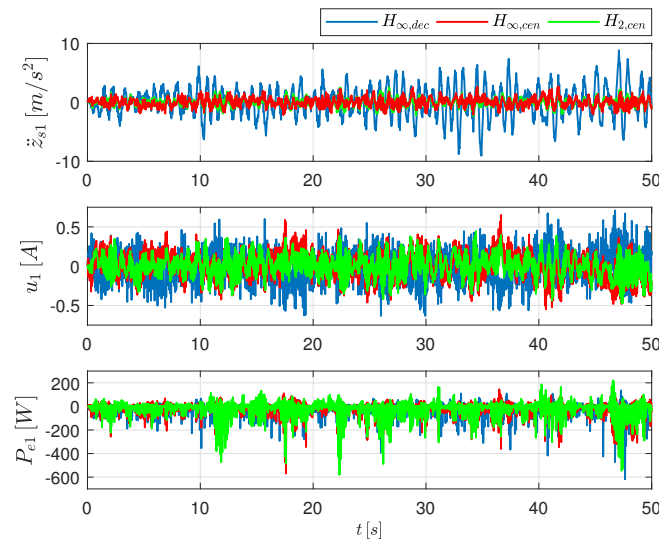


**Figure 6.** (top) Accelerations  $\ddot{z}_{s1}(t)$ , (middle) Actuation current  $i_1(t)$ , (down) Instantaneous harvested electrical power  $P_{e1}(t)$ .

4.2. Simulations for Ride Index = 0.47

In Table 2 the design knobs values used in the RI = 0.47 simulations are reported while the plots of the corresponding acceleration  $\ddot{z}_{s1}$ , actuation current  $i_1(t)$  and the electrical power  $P_{e1}(t)$  under the three control laws are reported in Figure 7.

**Table 2.** Knobs tuning—RI = 0.47.

RI = 0.47 (Trade-off between Comfort/Harvesting)				
Control	$\rho$	$\beta$	$\gamma$	$\alpha$
$H_{\infty,dec}$	0.323	100	10	42
$H_{\infty,cen}$	1.67	2.25	1	30
$H_{2,cen}$	0.82578	3.764	1	31

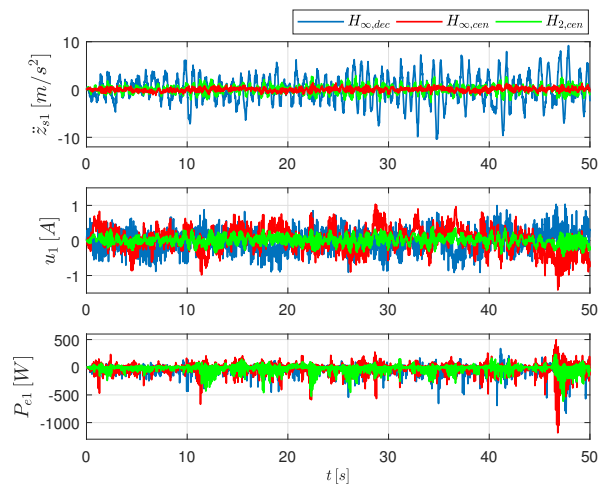


**Figure 7.** (top) Accelerations  $\ddot{z}_{s1}(t)$ , (middle) Actuation current  $i_1(t)$ , (down) Instantaneous harvested electrical power  $P_{e1}(t)$ .

4.3. Simulations for Ride Index = 0.70

Finally, in Table 3 the values of the design knobs used for the case RI = 0.70 are reported while the plots of the acceleration  $\ddot{z}_{s1}$ , actuation current  $i_1(t)$  and the harvested electrical power  $P_{e1}(t)$  under the three control laws are reported in Figure 8.

**Table 3.** Knobs tuning—RI = 0.70.

RI = 0.25 (Perceivable Discomfort/Largest Harvesting)				
Control	$\rho$	$\beta$	$\gamma$	$\alpha$
$H_{\infty,dec}$	0.42	100	10	47
$H_{\infty,cen}$	2.82	3	1	33
$H_{2,cen}$	2.167	4–69	1	33

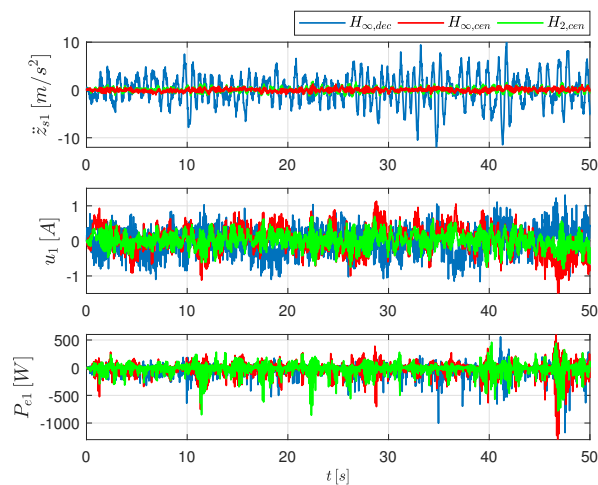


**Figure 8.** (top) Accelerations  $\ddot{z}_{s1}(t)$ , (middle) Actuation current  $i_1(t)$ , (down) Instantaneous harvested electrical power  $P_{e1}(t)$ .

#### 4.4. Average Harvested Electrical Power

Finally, next Table 4 summarize the average harvest electrical power during the simulations.

From the simulation it results that the  $H_{\infty, cen}$  and  $H_{2, cen}$  regulators, designated on the basis of the full-car suspension model, guarantee good rider performance and higher levels of harvested energy with respect to the  $H_{\infty, dec}$  controller in all the situations tested. Moreover, the ride comfort performance of the  $H_{\infty, dec}$  regulator, designated on the basis of the quarter-car suspension model and implemented in a decentralized way, degrades remarkably at the increase of the energy harvesting requirements. This can be seen from the accelerations  $\ddot{z}_{s1}(t)$  plots but similar conclusions can be drawn out by observing the sprung mass accelerations  $\ddot{z}_s(t)$  and the pitch and roll angles evolutions (non reported here for space limitations but available in [13]).

As far as the amount of harvested energy during the simulations, Table 4 allows one to observe that the centralized  $H_{\infty, cen}$  and  $H_{2, cen}$  regulators always are able to recover more energy than the decentralized  $H_{\infty, dec}$  controller, the more at lower values of the RI index. Moreover, it can be seen that the  $H_{2, cen}$  regulator recovers the largest amount of electric power, while the  $H_{\infty, cen}$  regulator is more robust in rejecting the exogenous signals acting to the system.

**Table 4.** Average harvest electrical power. The percentages express the improvements with respect to the  $H_{\infty, dec}$  control achievements for the same RI.

Average Harvest Electrical Power			
Control	RI = 0.25	RI = 0.47	RI = 0.70
$H_{\infty, dec}$	$4 \times 100$ W	$4 \times 124$ W	$4 \times 153$ W
$H_{\infty, cen}$	$4 \times 120$ W (+20%)	$4 \times 141$ W (+13%)	$4 \times 160$ W (+4.5%)
$H_{2, cen}$	$4 \times 141$ W (+40%)	$4 \times 154$ W (+24%)	$4 \times 168$ W (+10%)

### 5. Conclusions

The usage of regenerative suspension systems in modern electrical/hybrid cars could contribute to the vehicle’s autonomy with a modest degradation to the usual ride comfort and road handling performance. The integration of such systems with other existing energy harvesting devices, such as regenerative brakes, may help the diffusion of this kind of cars, providing together a total amount of many tens/hundreds watts.

This paper has complemented the results achieved in [3] on the design of active control laws for the regulation of regenerative suspension systems by extending the scalar MIPC approach there presented for a quarter-car system to the general multivariable solution achieved on the basis of a full-car model. Moreover, both the  $H_{\infty}$  and  $H_2$  state-feedback solutions have been considered based on a novel and *ad-hoc* state-space realization and have been shown to be enough flexible and powerful to easily trade-off amongst conflicting energetic and dynamic requirements.

From the simulations it results that the centralized solutions have to be preferred with respect to the decentralized one. In fact, from Table 4 it results that the improvements on the harvested energy are increasingly higher (up to 40% for the centralized  $H_2$  and up to 20% for the centralized  $H_{\infty}$  optimal controllers) as the ride index RI decreases. This is especially important in the large part of cars usage, where maintaining low values of the ride index is of paramount importance for ensuring a good ride comfort. It is also found that the centralized  $H_2$  control is able to gain the double of the energy harvested by the centralized  $H_{\infty}$  control for the same value of the ride index.

An important contribution of this work is the demonstration that the coordination of the control actions achievable by a multivariable design has to be preferred than a simpler decentralized

implementation. The usage of modern  $H_2$  and  $H_\infty$  multi-objective control design methodologies make the extra numerical complexity for the multivariable design negligible.

**Author Contributions:** Methodology, supervision and writing-review and editing A.C.; Investigation and formal analysis F.T.; Software, data curation, visualization and writing-original draft preparation P.V. All authors have read and agreed to the published version of the manuscript.

**Funding:** This research received no external funding.

**Conflicts of Interest:** The authors declare no conflict of interest.

## References

1. Abdelkareema, M.A.A.; Xua, L.; Alia, M.K.A.; Elagouza, A.; Mia, J.; Guoa, S.; Liuc, Y.; Zuoc, L. Vibration energy harvesting in automotive suspension system: A detailed review. *Appl. Energy* **2018**, *229*, 672–699. [[CrossRef](#)]
2. Zhang, R.; Wang, X.; John, S. A Comprehensive Review of the Techniques on Regenerative Shock Absorber Systems. *Energies* **2018**, *11*, 1167. [[CrossRef](#)]
3. Casavola, A.; di Iorio, F.; Tedesco, F.; Multiobjective, A.  $H_\infty$  Control Strategy for Energy Harvesting in Regenerative Vehicle Suspension Systems. *Int. J. Control* **2018**, *91*, 741–754. [[CrossRef](#)]
4. Casavola, A.; di Iorio, F.; Tedesco, F. Gain-scheduling control of electromagnetic regenerative shock absorbers for energy harvesting by road unevenness. In Proceedings of the 2014 IEEE American Control Conference, Portland, OR, USA, 4–6 June 2014.
5. Sultoni, A.I.; Sutantra, I.N.; Pramono, A.S.  $H_\infty$  Multi-Objective Implementation for Energy Control of Electromagnetic Suspension. *Int. Rev. Mech. Eng.* **2015**, *9*, 542–547. [[CrossRef](#)]
6. Kim, C.; Ro, P.I. An Accurate Full Car Ride Model Using Model Reducing Techniques. *J. Mech. Des.* **2002**, *124*, 697–705. [[CrossRef](#)]
7. Kecik, K.; Mitura, A.; Lenci, S.; Warminski, J. Energy harvesting from a magnetic levitation system. *Int. J. Non-Linear Mech.* **2017**, *94*, 200–206. [[CrossRef](#)]
8. Sammier, D.; Sename, O.; Dugard, L.  $H_\infty$  Control of Active Vehicle Suspensions. In Proceedings of the IEEE International Conference on Control Applications, Anchorage, AK, USA, 25–27 September 2000.
9. Poussot-Vassal, C.; Sename, O.; Dugard, L.; Gáspár, P.; Szabó, Z.; Bokor, J. A new semi-active suspension control strategy through LPV technique. *Control Eng. Pract.* **2008**, *16*, 1519–1534. [[CrossRef](#)]
10. ISO. ISO 2631-4: Human Exposure to Mechanical Vibration and Shock. Part 4: Guidelines for the Evaluation of the Effects of Vibration and Rotational Motion on Passenger and Crew Comfort in Fixed-Guideway Transport Systems; International Organization for Standardization: Geneva, Switzerland, 2001.
11. Chen, H.; Guo, K.H. Constrained Control of Active Suspensions: An LMI Approach. *IEEE Trans. Control Syst. Technol.* **2005**, *13*, 412–421. [[CrossRef](#)]
12. Rajamani, R. *Vehicle Dynamics and Control*, 2nd ed.; Springer: Berlin, Germany, 2012.
13. Vaglica, P. Modeling and Control of Regenerative Suspension Systems for Automobiles. Master's Thesis, University of Calabria, Rende, Italy, 2019.
14. Boyd, S.; El Ghaoui, L.; Feron, E.; Balakrishnan, V. *Linear Matrix Inequalities in System and Control Theory*; Society for Industrial and Applied Mathematics: Philadelphia, PA, USA, 1994; Volume 15.
15. ISO. ISO 8608:1995(E): Mechanical Vibration—Road Surface Profiles—Reporting of Measured Data; International Organization for Standardization: Geneva, Switzerland, 1995.



© 2020 by the authors. Licensee MDPI, Basel, Switzerland. This article is an open access article distributed under the terms and conditions of the Creative Commons Attribution (CC BY) license (<http://creativecommons.org/licenses/by/4.0/>).